Journal of Inorganic and General Chemistry
ZAAC
Zeitschrift für anorganische und allgemeine Chemie
www.zaac.wiley-vch.de
RESEARCH ARTICLE

Check for updates

DOI: 10.1002/zaac.202300199

Configuration of the dimolybdate in salt inclusion type of compounds, $Cs_2Mo_2O_7 \cdot CsX$ (X=Cl, Br, and I)

Anna Katharina Weber,[b] Ksenia Denisova,[c] Peter Lemmens,[d] and Angela Möller*[a]

Dedicated to Professor Michael Ruck on the occasion of his 60th birthday.

$Cs_2Mo_2O_7 \cdot CsI$ is obtained as a member of the series $Cs_2Mo_2O_7 \cdot CsX$ with X=Cl, Br, and I from the synthesis of Cs_2MoO_4 with MoO_3 and CsX. At room temperature, the compounds crystallize in the space group $P6_3/mmc$ with the dimolybdate, $[Mo_2O_7]^{2-}$, in a linear and eclipsed conformation. Low temperature Raman spectroscopy and low temperature X-ray diffraction were used to investigate the effect of the ${}^{2}_{\infty}\{CsX\}$ hetero-honeycomb lattice on the bridging angle of the dimolybdate. For X=Cl, a phase transition occurs below 150 K ($P6_3/mmc \rightarrow Cmcm$). The phase transition relates to a lock-in that involves bending of the (Mo–O–Mo) bridge. For the Pearson softer iodide compound, no phase transition is observed down to 4 K; thus, the linear configuration remains stable. Specific heat data and their evaluation in terms of phonon contributions are given.

Introduction

The alkaline-metal dimolybdates are actually adduct phases of the $A_2MoO_4 \cdot MoO_3$ type (A=K, Rb and Cs) and consist of $[MoO_4]^{2-}$ entities and neutral ${}^{1}_{\infty}\{MoO_{2/1}O_{2/2}\}$ chains. These compounds do not contain the motif of an isolated $[Mo_2O_7]^{2-}$ unit.[1–4] In contrast, $MgMo_2O_7$ presents an example for a bent dimolybdate (∠(Mo–O–Mo) = 160.7°) with an average deviation of 12.3° from the eclipsed conformation.[5] Compounds with $[Mo_2O_7]^{2-}$ units are scarce, e.g. $A_3Fe[MoO_4]_2[Mo_2O_7]$ with A=K,Cs.[6–8] In general, $[X_2O_7]^{n-}$ anions preferentially exist in a bent and staggered conformation, which has been extensively studied for the family of disilicates.[9] For X=P,[10,11] Cr,[12,13] V[13] and Ge[14] the different conformations D_{3d}, D_{3h}, and C_{2v}, respectively, were controversially discussed in terms of structural symmetry in relation to spectroscopic assignments of fundamental modes (IR/Raman).

Here, we are interested in a class of materials that belongs to the salt-inclusion type of compounds. These contain the ${}^{2}_{\infty}\{AX\}$ hetero-honeycomb layers which restrict the conformation of the dimolybdate, namely eclipsed and linear at room temperature. Members of this family of compounds, $A(1)_2Mo_2O_7 \cdot A(2)Cl$, with A(1) = Cs, Rb and A(2) = Cs, Rb, and K, were investigated in terms of cation sizes and Pearson hardness.[15] Previously, single crystal structures of $Cs_2Mo_2O_7 \cdot CsBr$[16] and $K_2Mo_2O_7 \cdot KBr$[17] have been reported and for the latter the Raman and IR bands of the dimolybdate were assigned based on D_{3h} symmetry.

Another example of an isotypic compound with a hetero honeycomb lattice and a linear divanadate in eclipsed conformation is $KBaV_2O_7 \cdot BaCl$.[18] The multianionic compounds $BaCu(OH)[V_2O_7] \cdot BaX$ with X=Cl, Br[19] crystallize in the space group *Pnma*, containing a bent divanadate (∠(V–O–V) ≈ 162°). However, the eclipsed conformation remains in this case as well. On the other hand, for cation-rich compounds such as $K_3YbSi_2O_7$, a phase transition from $P6_3/mmc$ to *Cmcm* at ≈210 K has been reported which establishes a bent disilicate (≈164°) in an eclipsed conformation.[20] The scope of the present work is to investigate the influence of the halide in the hetero-honeycomb lattice for the series $Cs_2Mo_2O_7 \cdot CsX$ with X=Cl, Br, and I with respect to the $[Mo_2O_7]^{2-}$ configuration by using low temperature X-ray diffraction and Raman spectroscopy.

Results and Discussion

The compounds $Cs_2Mo_2O_7 \cdot CsX$ with X=Cl, Br and I are obtained by reacting Cs_2MoO_4, MoO_3 with CsX in evacuated silica glass ampoules at temperatures of 823–873 K. The formation of $Cs_2Mo_2O_7 \cdot CsCl$ has been described in Ref. [15], following the reaction sequence: (a) Cs_2MoO_4 and MoO_3 react to form

[a] Prof. Dr. A. Möller
Department of Chemistry
Johannes Gutenberg-University Mainz
Duesbergweg 10–14, D-55128 Mainz (Germany)
E-mail: angela.moeller@uni-mainz.de
[b] A. K. Weber
Department of Chemistry
Johannes Gutenberg-University Mainz
Duesbergweg 10–14, D-55128 Mainz (Germany)
[c] Dr. K. Denisova
Institute for Condensed Matter Physics
TU Braunschweig
Mendelssohnstr. 3; D-38106 Braunschweig (Germany)
[d] Prof. Dr. P. Lemmens
Institute for Condensed Matter Physics
TU Braunschweig
Mendelssohnstr. 3, D-38106 Braunschweig (Germany)

© 2023 The Authors. Zeitschrift für anorganische und allgemeine Chemie published by Wiley-VCH GmbH. This is an open access article under the terms of the Creative Commons Attribution License, which permits use, distribution and reproduction in any medium, provided the original work is properly cited.

© 2023 The Authors. Zeitschrift für anorganische und allgemeine Chemie published by Wiley-VCH GmbH

$Cs_2MoO_4 \cdot MoO_3$ above 573 K, (b) formation of $Cs_2Mo_2O_7 \cdot CsX$ occurs in the melt (above 723 K). The latter reaction with the alkaline metal halide is exothermic for X=I (*m.p.* 775 K) and X=Cl (*m.p.* 830 K) whereas it is endothermic for X=Br (*m.p.* 835 K). Figure 1 shows the Rietveld refinements of powder X-ray diffraction data for $Cs_2Mo_2O_7 \cdot CsX$ with X=Cl, Br, and I at room temperature ($P6_3/mmc$) and at 150 K (X=Cl, *Cmcm*).

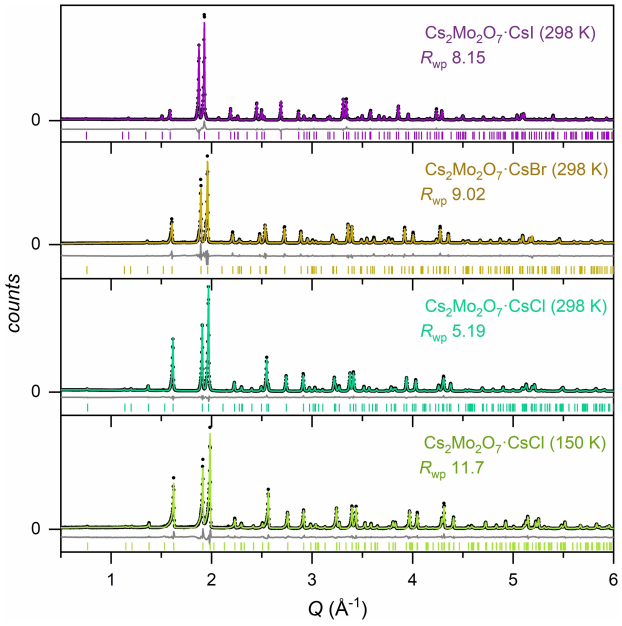

Figure 1. Rietveld refinement of powder diffraction data for $Cs_2Mo_2O_7 \cdot CsX$ with X=Cl, Br and I at room temperature and with X=Cl at 150 K. Experimental data are given in black circles and refinements by respective colored lines for X=Cl (green), Br (yellow), and I (purple). Gray lines represent the difference and colored bars the Bragg positions.

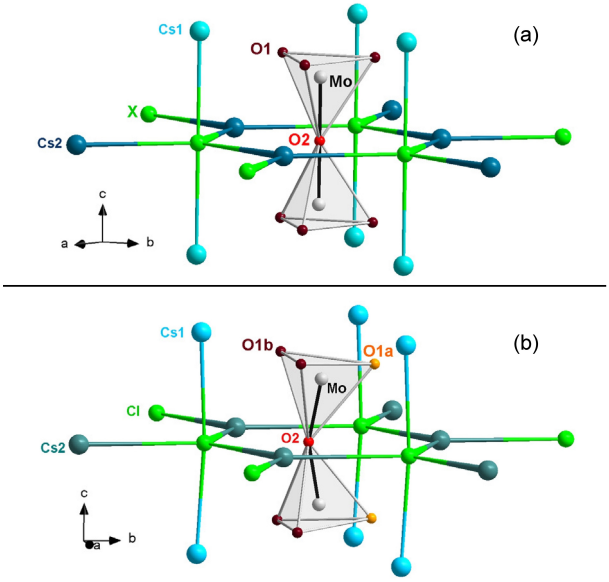

Figure 2. (a) Structural motifs ($P6_3/mmc$) of $Cs_2Mo_2O_7 \cdot CsX$ with X=Cl, Br and I. (b) $Cs_2Mo_2O_7 \cdot CsCl$ at 150 K (*Cmcm*) with bent dimolybdate units.

As synthesized $Cs_2Mo_2O_7 \cdot CsX$ with X=Cl, Br, and I crystallize in the space group $P6_3/mmc$ with two formula units per unit cell. The structure consists of two motifs with disparate dimensionalities (see Figure 2a): (i) The $^2_\infty\{Cs2X\}$-hetero-honeycomb lattice with additional apical Cs1 resulting in a trigonal-bipyramidal coordination of the halide, and (ii) the dimolybdate $[Mo_2O_7]^{2-}$ with the bridging oxygen atom (O2) located in the center of the {Cs2X}-hexagons. Room temperature structural data for all three compounds reveal a rare eclipsed conformation for $[Mo_2O_7]^{2-}$ (D_{3h} symmetry) with a linear Mo–O2–Mo bridge. While the apical Cs1 cations restrict the rotation of the dimolybdate towards a staggered conformation, the electrostatic interaction between O2 and the hetero-honeycomb forming ions may allow for a distortion towards bending. Here, we focus on the halides with different sizes (MEFIR-MEan Fictive Ionic Radii:[21] $r_{Cl}=173$ pm,[15] $r_{Br}=185$ pm, $r_I=202$ pm) and Pearson hardness.[22] In other words, the question arises how restrictive is the honeycomb lattice with respect to distortion and consequently a structural transition.

Low-temperature powder diffraction data (100–300 K) for the two border cases with X=Cl and I reveal that the thermal expansion coefficients are negative along [001] (α_c) and positive for α_a. The former values are about three times larger for X=Cl ($\alpha_c \approx -3 \cdot 10^{-6}$ K^{-1}) compared to X=I ($\alpha_c \approx -1 \cdot 10^{-6}$ K^{-1}), whereas $\alpha_a \approx 4.5 \cdot 10^{-5}$ K^{-1} reflects the softness of the $^2_\infty\{Cs2X\}$-hetero-honeycomb lattice.

We used a pseudo-hexagonal setup of the cell ($b' = \sqrt{3}a$) to evaluate the phase transition from $P6_3/mmc$ to *Cmcm*. Only for X=Cl the orthorhombic lattice parameter, b', exceeds significantly the expected one based on the hexagonal structure. Thus, the low-temperature structure (*Cmcm*, $a=6.3239(2)$, $b=10.9613(4)$, $c=16.3972(2)$ Å, and $V=1136.63(5)$ Å^3, $Z=4$) is established below 150 K for $Cs_2Mo_2O_7 \cdot CsCl$, see also Figure 1 and Scheme 1.

In more details, tilting of the MoO_3-units lead to an increase in Cs1–O1a (decrease in Cs1–O1b) distances along [001] upon cooling corresponding to a negative α_c and a compression of the hexagon related to the in-plane displacement of O2 (Figure 2b). Thus, the $[Mo_2O_7]^{2-}$ unit becomes bent with ∠(Mo–O2–Mo) ≈ 159°. In the course of the transition, the in-plane angles of the {Cs2X}-hexagon deviate from 120° by 4°. It should be noted that the Mo–Mo distance remains almost unchanged within experimental error over the entire temper-

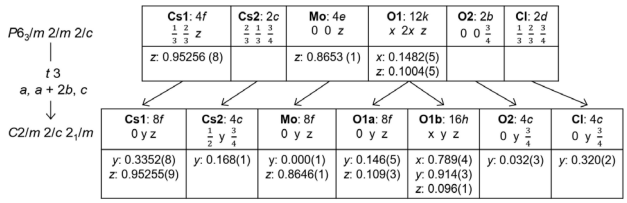

Scheme 1. Bärnighausen tree with group-subgroup relation of $P6_3/mmc$ and *Cmcm*.

© 2023 The Authors. Zeitschrift für anorganische und allgemeine Chemie published by Wiley-VCH GmbH

15213749, 0, Downloaded from https://onlinelibrary.wiley.com/doi/10.1002/zaac.202300199 by Universitätsbibliothek Mainz, Wiley Online Library on [06/12/2023]. See the Terms and Conditions (https://onlinelibrary.wiley.com/terms-and-conditions) on Wiley Online Library for rules of use; OA articles are governed by the applicable Creative Commons License

15213749, 0, Downloaded from https://onlinelibrary.wiley.com/doi/10.1002/zaac.202300199 by Universitätsbibliothek Mainz, Wiley Online Library on [06/12/2023]. See the Terms and Conditions (https://onlinelibrary.wiley.com/terms-and-conditions) on Wiley Online Library for rules of use; OA articles are governed by the applicable Creative Commons License

ature range down to 100 K. Therefore, bending gives rise to a slight increase in *d*(Mo–O2) of approximately 2.3(8) pm.

While for $Cs_2Mo_2O_7 \cdot CsCl$ the X-ray diffraction data in the entire temperature range were well fitted using the space group *Cmcm*, this was not the case for $Cs_2Mo_2O_7 \cdot CsI$. In particular, the elongation along [001] and the distortion of the hetero-honeycomb (less than 2°) was within the experimental error. Therefore, we choose Raman spectroscopy as a local probe to investigate whether a symmetry reduction occurs from the D_{3h} point group to the bent configuration (C_{2h}) of the dimolybdate.

We start the spectroscopic considerations from a group theoretical analysis of the optical modes in the space group $P6_3/mmc$. In total 17 modes are Raman active ($4A_{1g}+8E_{2g}+5E_{1g}$). The atoms localized on a mirror plane are characterized by an E_{2g} mode, only. This applies to Cs2 (2*c*) and X (2*d*) sites, which form the hetero-honeycomb lattice, as well as the bridging oxygen (O2, 2*b*). The apical Cs1 (4*f*) and Mo (4*e*) located along the *c*-axis give rise to three modes (A_{1g}, E_{1g}, and E_{2g}) each. The O1 site (12*k*), which presents the six terminal oxygen of the $[Mo_2O_7]^{2-}$ unit, correspond to two A_{1g}, three E_{1g}, and three E_{2g} modes. While E_{1g} modes are usually of very low intensity in backscattering geometry, we are concerned only with the assignments of the A_{1g} and E_{2g} modes with significant intensities here. In order to distinguish the latter two, polarized single crystal spectra in xx- and xy-backscattering geometry (xx: A_{1g} and E_{2g} and xy: only E_{2g}) are evaluated. Polarized Raman spectra of a $Cs_2Mo_2O_7 \cdot CsI$ single crystal are shown in Figure 3 for two single crystal orientations providing additional information on depolarized modes as well. In total, we observe $4A_{1g}$ and $8E_{2g}$ modes.

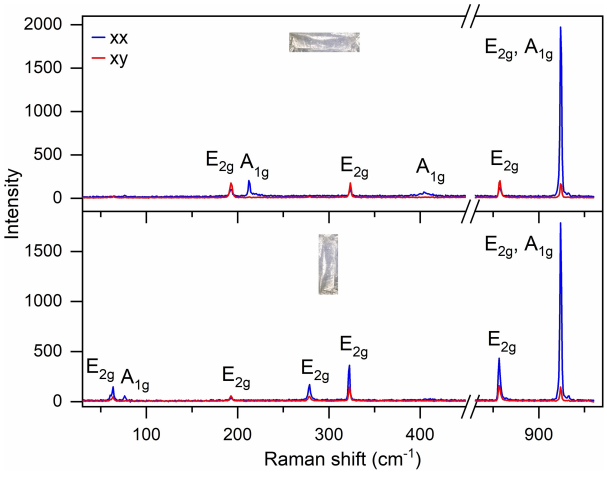

Figure 3. Single crystal Raman spectra of $Cs_2Mo_2O_7 \cdot CsI$ at 4 K. The insets show microscopic graphs of the single crystal with an elongated morphology in two different orientations. The incident Laser polarization is vertically polarized.

Vibrations of the individual atoms from their crystallographic sites are assigned to peak frequencies listed in Table 1. We start with O1 (12*k*) representing the terminal oxygen of the dimolybdate. Above 850 cm^{-1} the three fundamental stretching modes are observed for this complex oxide. The interatomic distance, Mo–O1, obtained from X-ray data corresponds well with the observed frequency of the A_{1g} mode according to an empirical model for molybdates.[23,24] The mode around 330 cm^{-1} is assigned to the symmetric deformation by three O1 within the MO_3-unit, while the one around 405 cm^{-1} represents the displacement of all six O1 of the dimolybdate along [001], respectively.

Next, we focus on the bridging O2 (2*b*). Only one E_{2g} mode is expected for a linear {Mo–O2–Mo} entity in the case of $Cs_2Mo_2O_7 \cdot CsI$ and is assigned to the bending vibration occurring around at 280 cm^{-1}. The displacement of Mo is observed at 213 cm^{-1} and corresponds to the symmetric (depolarized) stretching mode of the linear {Mo–O2–Mo} entity (Figure 3). The corresponding (deformation) lattice mode E_{2g} (Mo, 4*e*) is assigned to 63 cm^{-1}.

All other modes below 200 cm^{-1} are inherently linked to vibrations occurring within the Cs–X lattice. Since Cs2 and I form the hetero-honeycomb lattice with only one Raman-active E_{2g} mode each, we assign the mode at 193 cm^{-1} to a combined in-plane distortion. It is noteworthy, that the $^2_\infty\{Cs2X\}$-net is formally neutral and therefore the electrostatic interaction of X with the apical Cs1 can be considered as dominated by dipolar interactions which are presumably decoupled. Thus, the enhanced ionic character of Cs1 would act mainly as a counterbalance of the charged dimolybdate ions. Hence, the two modes at the lowest frequency energies (61 and 76 cm^{-1}) relate to principle displacements of Cs1. According to the selection rules of the polarized spectra (Figure 3) these are of E_{2g} and A_{1g} character.

Table 1. Assignment of Raman modes for $Cs_2Mo_2O_7 \cdot CsX$ (space group $P6_3/mmc$) with principal displacements related to the atom site.

site	A_{1g} [a]	E_{2g} [a]	A_{1g} [b]	E_{2g} [b]	A_{1g} [c]	E_{2g} [c]
O1	924	924	928	928	929	929
	405	857	~405	862	~410	866
		323		331		332
O2	–	279	–	286	–	absent
Mo	213	63	absent	70	absent	absent
Cs1	76	61	75	61	73	59
Cs2/X	–	193	–	200	–	201

[a] Single crystal Raman data for $Cs_2Mo_2O_7 \cdot CsI$ at 4 K. [b] Powder Raman data for $Cs_2Mo_2O_7 \cdot CsBr$ at 300 K. [c] Powder Raman data for $Cs_2Mo_2O_7 \cdot CsCl$ at 300 K.

© 2023 The Authors. Zeitschrift für anorganische und allgemeine Chemie published by Wiley-VCH GmbH

15213749, 0, Downloaded from https://onlinelibrary.wiley.com/doi/10.1002/zaac.202300199 by Universitätsbibliothek Mainz, Wiley Online Library on [06/12/2023]. See the Terms and Conditions (https://onlinelibrary.wiley.com/terms-and-conditions) on Wiley Online Library for rules of use; OA articles are governed by the applicable Creative Commons License

In the following, we discuss the selection criteria for combinations of the lattice modes: (i) the A_{1g}(Mo) is observed along the [001]-direction of the single crystal, while E_{2g}(O2) is absent and vice versa for the orthogonal crystal mounting, and (ii) all modes corresponding to the frequency energy 50 to 100 cm^{-1} (Cs1) are only of significant intensity when polarized by the in-plane O2-displacement. This implies that the Raman spectra of powder data (Figure 4) may exhibit disparate intensities.

In Figure 4 (top) we compare the powder Raman spectra of $Cs_2Mo_2O_7 \cdot CsX$ with X=Cl, Br and I at 300 K. The intensities were normalized to the highest mode at $\approx$ 930 cm^{-1}. The assignment for the iodide-compound (single-crystal) are listed for comparison together with the powder data for X=Cl and Br, in Table 1.

At room temperature a red shift of up to 8 cm^{-1} is observed from X=Cl to I for all modes. This corresponds to the Pearson softer and larger halides. Only the Cs1 lattice modes are slightly blue shifted. The most prominent features are the vanishing intensity of E_{2g} (O2 and Mo) for X=Cl which clearly mark the locking-in from a dynamical pseudo-linear {Mo–O2-Mo}-unit to a static bent one. We attribute this to the phase transition from $P6_3/mmc$ to *Cmcm*. In more detail, we compare the temperature dependence of $Cs_2Mo_2O_7 \cdot CsX$ with X=Cl and I in Figure 4. The absence of E_{2g}(O2) for X=Cl at around 280 cm^{-1} and the concomitant intensities of 3+1 modes around 220 cm^{-1} provide intriguing evidence for the symmetry reduction occurring sluggishly upon lower temperatures. A symmetry reduction into the space group *Cmcm* results in the transformation of the E_{2g} modes into one A_g and one B_{1g} mode each, while the A_{1g} modes transform into A_g modes. The transformation of the E_{1g} mode into a B_{2g} and a B_{3g} mode can be neglected due to the too low intensity in back scattering geometry. We assign the mode at 200 cm^{-1} to the combination frequency of the honeycomb lattice Cs2-X with A_g character. The two additional modes with the same intensity at 216 cm^{-1} and 220 cm^{-1} can accordingly be assigned to the added B_{1g} modes. For the bent molybdate unit, the A_g mode at 225 cm^{-1} and the B_{1g} mode at 238 cm^{-1} are observed for the displacement of the bridging oxygen O2. The deformation frequency is, as expected, lower for the bent configuration than for the linear configuration.[25] Due to the activity of O2, the modes for Mo1 are inactive as described before.

The appearance of two modes around 410 cm^{-1} is well in line with a bent dimolybdate as it shows lifting of the total symmetric deformation arising from the displacement of all six O1 along [001] in $P6_3/mmc$. Following the symmetry reduction at lower temperatures O1a' (8*f*) and O1b' (16*h*), this will lead each to two main modes A_g and B_{1g}.

Insights into the interaction of the dimolybdate with the hetero-honeycomb lattice in stabilizing either the linear or the bent configuration are evaluated further. In Figure 5, we show the temperature dependent frequencies, line widths (FWHM), and integral intensities of selected modes. The Mo–O stretching frequency at about 860 cm^{-1} exhibits a typical increase in energy towards low temperatures and settles to a constant value below 150 K. The deformation mode at about 330 cm^{-1} shows a softening with decreasing temperature, with a step around 150 K for X=Cl. The line widths are comparable for X=Cl and I below 150 K. However, the intensities are twice as large for the iodine over the entire temperature range. This corresponds to higher polarizabilities.

Contrary, the interactions within the plane are different. Again, softening with decreasing temperatures for both cases is

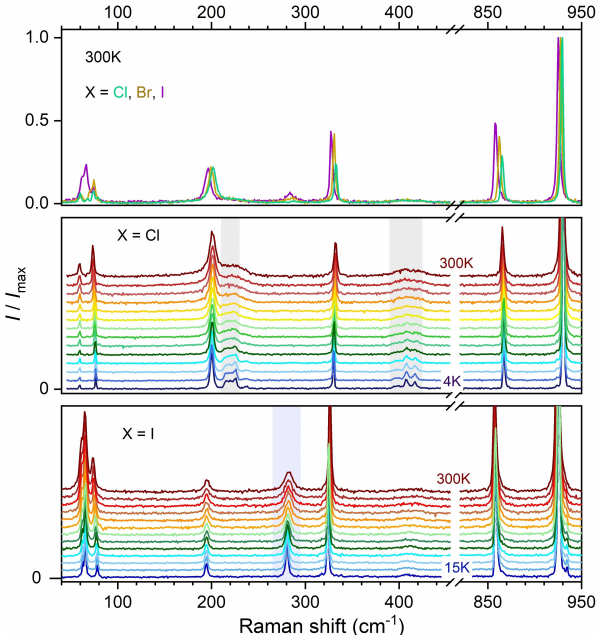

Figure 4. Top: Raman spectra of powder samples of $Cs_2Mo_2O_7 \cdot CsX$ with X=Cl, Br, and I at 300 K. Middle: Temperature-dependent Raman spectra of $Cs_2Mo_2O_7 \cdot CsCl$. Bottom: Temperature-dependent Raman spectra of $Cs_2Mo_2O_7 \cdot CsI$. The individual spectra at low temperatures are shown with an offset. Shaded areas mark the main differences discussed in the text.

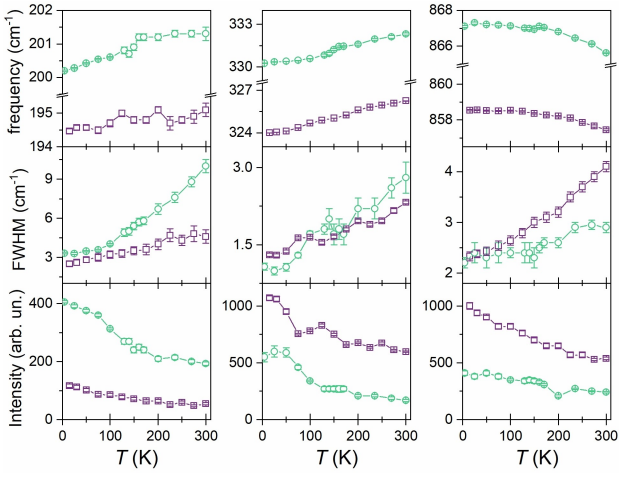

Figure 5. Frequency, line width (FWHM) and intensity for the Lorentzian fits at about 200 cm^{-1}, 330 cm^{-1} and 860 cm^{-1} of the low temperature Raman spectra of $Cs_2Mo_2O_7 \cdot CsX$ with X=Cl (green dots) and I (purple squares).

© 2023 The Authors. Zeitschrift für anorganische und allgemeine Chemie published by Wiley-VCH GmbH

observed for the {Cs2X}-mode at about 200 cm^{-1}. More intriguing is the increasing linewidth with temperature above the inflection point at 100 K. Here the FWHM value for X=Cl exceeds the one for iodine by a factor of up to three, which points to the larger structural instability. Note, that the intensities for X=Cl are larger than the observed ones for iodine by a factor of two.

Measurements of the heat capacity are used to provide further insights into the lattice dynamics and to search for related instabilities. The experimental C_p/T data for the two border cases X=Cl and X=I is shown in Figure 6. The thermodynamic data were fitted to a combined Debye-Einstein model in the temperature range from 2 to 300 K. For further details, we refer to Scheme 2, Table 2, and the experimental section. The total number of modes was fixed to three times the total number of atoms per formula unit ($3n_{f.u.} = n_{total} = 39$) corresponding to the high-temperature limit of $3n_{f.u.}R$ (Dulong-Petit law, with the gas constant R).

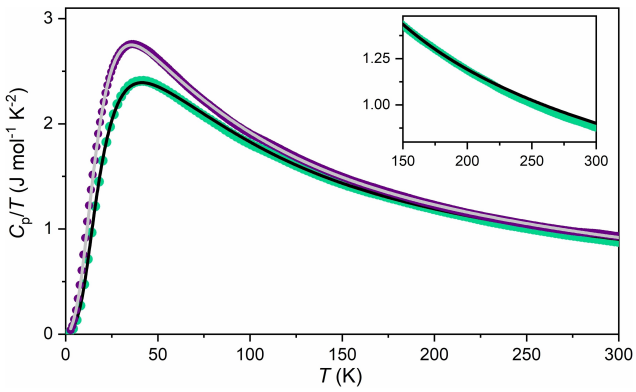

Figure 6. Heat capacity measurement data of $Cs_2Mo_2O_7 \cdot CsX$ with X=Cl (green) and I (purple) circles. Lines represent the respective combined Einstein-Debye model used; see also Table 2 and Scheme 2. The inset shows the deviation at high temperatures for X=Cl.

$$D(\theta_D) = 3R\left(\frac{T}{\theta_D}\right)^3 \int_0^{\theta_D/T} \frac{x^4 e^x}{(e^x-1)^2} dx \quad (1)$$

$$E_i(\theta_{E_i}) = R\left(\frac{\theta_{E_i}}{T}\right)^2 \exp\left(\frac{\theta_{E_i}}{T}\right)\left[\exp\left(\frac{\theta_{E_i}}{T}\right)-1\right]^{-2} \quad (2)$$

$$n_4 = n_{total} - n_D - \sum_{i=1}^{3} n_i \quad (3)$$

$$C_p(T) = n_D D(\theta_D) + \sum_{i=1}^{4} n_i E_i(\theta_{E_i}) \quad (4)$$

Scheme 2. Debye (1) and Einstein (2) functions, number of lattice modes (3), and fit model for the specific heat (4).

We used one Debye (Θ_D) and four Einstein (Θ_{E1-4}) temperatures, with $\Theta_{E3,4}$ relating to the high energy/high temperature fundamental modes of the $[Mo_2O_7]^{2-}$. Our derived Θ_{E2-4} values are similar to those reported for $Cs_2MoO_4 \cdot MoO_3$[4] while the fits based on two Einstein temperatures for the molybdates listed in[26] significantly differ. In conclusion, we suggest that Θ_{E2} is sensitive to the counter ion (here Cs^+) while $\Theta_{E3} \approx 330$ K and $\Theta_{E4} \approx 950$ K are molybdate related and may be used for orthomolybdates in general.

However, the differences between the chloride and iodide compounds are evident at lower temperatures where lattice modes mainly associated with the displacements of Cs1 and {Cs2X} dominate. The respective temperatures ($\Theta_{D,\,E1,2}$) obtained from our fit show an average shift of approximately −15 K for the iodide compound respective to the chloride. The interesting aspect is the comparatively large difference in Debye temperatures in relation to the highest Einstein modes (fundamental Mo–O stretching frequencies). This explains phenomenological the phonon softening observed for selected lower energy optical modes in relation to the acoustic ones.

The inset of Figure 6 shows the developing difference between the experimental data for X=Cl and our model above the phase transition, while the entire temperature range is reasonably fitted for X=I. We integrated the difference (fit-experiment), $\Delta C_p(T)$, in the temperature range from 175 K to 300 K for X=Cl and obtained $\Delta H \approx 0.45$ kJ/mol, presumably associated with the gradual phase transition $P6_3/mmc \leftrightarrow Cmcm$.

Conclusions

$CsMo_2O_7 \cdot CsX$ with X=Cl, Br, and I were synthesized and characterized by powder X-ray diffraction. The structure contains isolated dimolybdate units well separated by $^2_\infty\{CsX\}$ hetero-honeycomb layers. We found a structural transition for X=Cl around 150 K from $P6_3/mmc$ to $Cmcm$ upon cooling. Concomitantly, bending of the dimolybdate occurs. In order to gain deeper understanding of the differences between the

Table 2. Model parameters (temperatures in K and number of modes) from the combined Debye-Einstein model for the heat capacity data of $Cs_2Mo_2O_7 \cdot CsX$ with X=Cl and I.

X	Θ_{D1} n_{D1}	Θ_{E1} n_{E1}	Θ_{E2} n_{E2}	Θ_{E3} n_{E3}	Θ_{E4} n_{E4}
Cl	78	86	149	332	948
	3.0[a]	*8.3*	*8.9*	*8.8*	*10.0*
I	64	78	127	335	936
	3.0[a]	*8.3*	*9.3*	*9.6*	*8.8*

[a] Fixed value.

© 2023 The Authors. Zeitschrift für anorganische und allgemeine Chemie published by Wiley-VCH GmbH

15213749, 0, Downloaded from https://onlinelibrary.wiley.com/doi/10.1002/zaac.202300199 by Universitätsbibliothek Mainz, Wiley Online Library on [06/12/2023]. See the Terms and Conditions (https://onlinelibrary.wiley.com/terms-and-conditions) on Wiley Online Library for rules of use; OA articles are governed by the applicable Creative Commons License

15213749, 0, Downloaded from https://onlinelibrary.wiley.com/doi/10.1002/zaac.202300199 by Universitätsbibliothek Mainz, Wiley Online Library on [06/12/2023]. See the Terms and Conditions (https://onlinelibrary.wiley.com/terms-and-conditions) on Wiley Online Library for rules of use; OA articles are governed by the applicable Creative Commons License

former and the iodide derivate we evaluated the low-temperature Raman spectra on powders and polarized single-crystals.

From the thermodynamic point of view, the peculiarity of the $CsMo_2O_7{\cdot}CsX$ compounds lie in the rather small Debye and large range of Einstein mode frequencies. This decouples the higher energy optical phonons (M–O) effectively from scattering processes (anharmonicities). Therefore, the optical phonon anomalies probed by Raman scattering are more pronounced for the lower frequency phonons, e.g. the in-plane displacement within the {Cs–X} hetero-honeycomb layer. Worth mentioning is that in this case (mode around 200 cm^{-1}) the inflection point ($\approx$100 K) of the line width for X=Cl corresponds roughly to the Debye temperature and is not identical with the phase transition temperature around 150 K. This indicates that the optical phonons themselves do not promote the first order structural phase transition. The observed phonon softening is therefore mainly resulting via multi-phonon decay processes from optical to acoustic modes. However, such anomalous effects are more pronounced for X=Cl and quite moderate for X=I.

At around 150 K the step in mode frequencies is in line with the phase transition also determined from X-ray diffraction for X=Cl and supported by Raman spectra. No phase transition is observed for X=I. In conclusion, the Pearson softer iodide suppresses the bent configuration of the dimolybdate. More so, the related linear Mo–O2–Mo mode exists down to 4 K, whereas this mode is absent for X=Cl which serves as a suitable hallmark to distinguish the differences in configuration of the dimolybdate.

Experimental Section

Starting materials were synthesized from Cs_2CO_3 (99%, Alfa Aesar) and MoO_3 (99.9+ %, ChemPur, fine chemicals): Cs_2MoO_4 at 600 °C for 48 h in corundum crucibles, CsBr was synthesized by dissolving Cs_2CO_3 in diluted HBr (48 wt-%, Alfa Aesar) and subsequent drying. $Cs_2Mo_2O_7{\cdot}CsX$ with X=Cl, Br and I were synthesized in evacuated silica glass ampoules (p ~$2{\cdot}10^{-2}$ mbar) from Cs_2MoO_4, MoO_3 and CsCl ($\geq$98%, Sigma) or CsI (99.99%, ChemPur, fine chemicals) at 550 °C, or CsBr at 600 °C for 6 h. Single crystals of $Cs_2Mo_2O_7{\cdot}CsI$ grew in the shape of plates directly from the melt.

Thermal analysis (DTA/TG) measurements were carried out on a STA 449 Jupiter F3 (Netzsch) with a heating and cooling rate of 10 °C/min from 25 to 610 °C for X=Br and up to 550 °C for X=I in corundum crucibles under an argon gas flow of 25 mL/min.

The samples were characterized by Rietveld refinements[27] of X-Ray diffraction data (STOE Stadi P; STOE & Cie, transmission geometry, Mo $K\alpha_1$, Dectris MYTHEN 1 K detector) using polyvinyl acetate (PVAC) foils on a flat sample holder. External calibration (LaB_6 standard) and capillary measurements (diameter 0.3 mm, thickness 0.01 mm) for the internal zero-point correction of the lattice constants were applied. A capillary measurement for $Cs_2Mo_2O_7{\cdot}CsBr$ was used for the Rietveld refinement. Low temperature X-ray diffraction experiments were performed in capillaries. A cryogenic head (Cryostream800, Oxford Instruments) with liquid nitrogen was used in the temperature range from 100 K to 340 K, 10 K steps, cooling rate 6 K/min and 4 min hold during measurement.

Raman scattering experiments were performed with a Jobin Yvon LabRam HR800 Micro Raman spectrometer with a 50x-objective. The spectra were collected in quasi-backscattering geometry using a $\lambda = 532$ nm laser line of a Nd:YAG laser with a power of 30 μW. Low temperature data were collected with the samples inserted in a CryoVac, He-cooled micro-cryostat in the temperature range from 4 to 300 K in an energy range from 10 to 1300 cm^{-1}.

The specific heat measurement were performed with a cryogen-free Physical Property Measurement System (PPMS DynaCool 9, Quantum Design) by using the heat capacity option in zero field and the temperature range from 300 K to 2 K. Corrections to the data (puck and Apizon grease) were applied by measuring an addendum before starting the sample measurement of the respective pressed pellet.

Evaluation of the specific heat data (software OriginPro 2019, Levenberg Marquardt iteration algorithm): The model parameters listed in Table 2 were obtained from fits to a combined Debye-Einstein model, see Scheme 2. Note that the fits reported in [4] and [26] are on number of atoms per formula unit and often deviate from the total number of atoms per formula unit and the theoretical number of acoustic modes. Therefore, we used a modified constrained fit of Cp/T data based on: $n_{E4} = 3n_{f.u.} - n_D - n_{E1} - n_{E2} - n_{E3}$ and fixed $n_D = 3$. The initial Debye temperatures were obtained from a linear fit to Cp/T versus T^2. The standard deviation of all listed (Θ_D, Θ_{E1-3}) temperatures is less than $\pm$3 K and for Θ_{E4} 940 $\pm$ 10 K while the number of Einstein modes given are reliable within $\pm$0.1.

Structural and optical mode analysis were carried out using programs provided by the Bilbao crystallographic server.[28–30]

Acknowledgements

The support from the German Research Foundation (Deutsche Forschungsgemeinschaft, DFG) under the projects 443703006 CRC 1487 and 442589410 is gratefully acknowledged. PL and KD acknowledge support from DFG-RTG 1952 and EXC-2123 Quantum Frontiers – 390837967. Open Access funding enabled and organized by Projekt DEAL.

Conflict of Interest

The authors declare no conflict of interest.

Data Availability Statement

The data that support the findings of this study are available from the corresponding author upon reasonable request.

Keywords: Halides · Molybdates · Phase Transition · Raman Spectroscopy

[1] E. S. Zolotova, S. F. Solodovnikov, Z. A. Solodovnikova, V. N. Yudin, N. F. Uvarov, A. S. Sukhikh, *J. Phys. Chem. Solids* **2021**, *154*, No. 110054.
[2] S. A. Magarill, R. F. Klevtsova, *Sov. Phys. Crystallogr.* **1972**, *16*, 645.

© 2023 The Authors. Zeitschrift für anorganische und allgemeine Chemie published by Wiley-VCH GmbH

[3] Z. A. Solodovnikova, S. F. Solodovnikov, *Acta Crystallogr. Sect. C* **2006**, *62*, i53–i56.
[4] A. L. Smith, G. Kauric, L. van Eijck, K. Goubitz, G. Wallez, J.-C. Griveau, E. Colineau, N. Clavier, R. J. M. Konings, *J. Solid State Chem.* **2017**, *253*, 89–102.
[5] K. Stadnicka, J. Haber, R. Kozlowski, *Acta Crystallogr. Sect. B* **1977**, *33*, 3859–3862.
[6] M. Mączka, A. Pietraszko, W. Paraguassu, A. G. Souza Filho, P. T. C. Freire, J. Mendes Filho, J. Hanuza, *J. Phys. Condens. Matter* **2009**, *21*, 095402.
[7] A. Souilem, M. F. Zid, A. Driss, *Acta Crystallogr. Sect. E* **2014**, *70*, i38.
[8] K. M. Khal'baeva, S. F. Solodovnikov, E. G. Khaikina, Y. M. Kadyrova, Z. A. Solodovnikova, O. M. Basovich, *J. Solid State Chem.* **2010**, *183*, 712–719.
[9] F. Liebau, *Structural Chemistry of Silicates: Structure, Bonding and Classification*, Springer-Verlag, Berlin, **1985**.
[10] A. Hezel, S. D. Ross, *Spectrochim. Acta Part A* **1967**, *23*, 1583–1589.
[11] R. W. Mooney, R. L. Goldsmith, *J. Inorg. Nucl. Chem.* **1969**, *31*, 933–942.
[12] H. Stammreich, D. Bassi, O. Sala, H. Siebert, *Spectrochim. Acta* **1958**, *13*, 192–196.
[13] R. G. Brown, S. D. Ross, *Spectrochim. Acta Part A* **1972**, *28*, 1263–1274.
[14] P. Tarte, M. J. Pottier, A. M. Procès, *Spectrochim. Acta Part A* **1973**, *29*, 1017–1027.
[15] A. K. Weber, M. Panthöfer, A. Möller, *Inorg. Chem.* **2022**, *61*, 10108–10115.
[16] A. S. Pakhomova, S. V. Krivovichev, *Acta Crystallogr. Sect. E* **2009**, *65*, i87.
[17] H. J. Becher, H.-J. Brockmeyer, U. Prigge, *J. Chem. Res. Miniprint* **1978**, 1670–1682.
[18] F.-D. Martin, Hk. Müller-Buschbaum, *Z. Naturforsch.* **1994**, *49b*, 1141–1144.
[19] K. Sun, A. P. Litvinchuk, J. Tapp, A. Möller, *J. Solid State Chem.* **2016**, *236*, 69–77.
[20] P. Dabić, V. Kahlenberg, B. Krüger, M. Rodić, S. Kovač, J. Blanuša, Z. Jagličić, L. Karanović, V. Petříček, A. Kremenović, *Acta Crystallogr. Sect. B* **2021**, *77*, 584–593.
[21] R. Hoppe, *Z. Kristallogr.-Crystallogr. Mater.* **1979**, *150*, 23–52.
[22] R. G. Pearson, *J. Am. Chem. Soc.* **1963**, *85*, 3533–3539.
[23] F. D. Hardcastle, I. E. Wachs, *J. Raman Spectrosc.* **1990**, *21*, 683–691.
[24] F. A. Cotton, R. M. Wing, *Inorg. Chem.* **1965**, *4*, 867–873.
[25] J. Weidlein, U. Müller, K. Dehnicke, *Schwingungsspektroskopie: Eine Einführung*, 2nd ed., Stuttgart, Georg Thieme Verlag, **1988**, p.53.
[26] E. Gamsjäger, M. Wiessner, *Monatsh. Chem.* **2018**, *149*, 357–368.
[27] A. A. Coelho, *TOPAS-Academics-64 V7.14*, Topas, 2020.
[28] E. Kroumova, M. I. Aroyo, J. M. Perez Mato, A. Kirov, C. Capillas, S. Ivantchev, H. Wondratschek, *Phase Transit.* **2003**, *76*, 155–170.
[29] M. I. Aroyo, J. M. Perez-Mato, D. Orobengoa, E. Tasci, G. de la Flor, A. Kirov, *Bulg. Chem. Commun.* **2011**, *43*, 183–197.
[30] S. Ivantchev, E. Kroumova, G. Madariaga, J. M. Perez-Mato, M. I. Aroyo, *J. Appl. Crystallogr.* **2000**, *33*, 1190–1191.

Manuscript received: September 20, 2023
Revised manuscript received: October 24, 2023
Accepted manuscript online: October 26, 2023

© 2023 The Authors. Zeitschrift für anorganische und allgemeine Chemie published by Wiley-VCH GmbH

15213749, 0, Downloaded from https://onlinelibrary.wiley.com/doi/10.1002/zaac.202300199 by Universitätsbibliothek Mainz, Wiley Online Library on [06/12/2023]. See the Terms and Conditions (https://onlinelibrary.wiley.com/terms-and-conditions) on Wiley Online Library for rules of use; OA articles are governed by the applicable Creative Commons License

RESEARCH ARTICLE

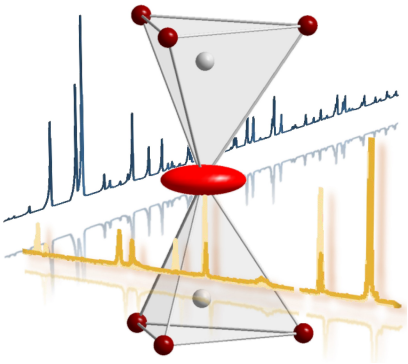

*A. K. Weber, Dr. K. Denisova, Prof. Dr. P. Lemmens, Prof. Dr. A. Möller**

1 – 8

Configuration of the dimolybdate in salt inclusion type of compounds, $Cs_2Mo_2O_7 \cdot CsX$ (X=Cl, Br, and I)

15213749, 0, Downloaded from https://onlinelibrary.wiley.com/doi/10.1002/zaac.202300199 by Universitätsbibliothek Mainz, Wiley Online Library on [06/12/2023]. See the Terms and Conditions (https://onlinelibrary.wiley.com/terms-and-conditions) on Wiley Online Library for rules of use; OA articles are governed by the applicable Creative Commons License